Inorganic Chemistry

ARTICLE

pubs.acs.org/IC

Scandium Ion-Enhanced Oxidative Dimerization and *N*-Demethylation of *N*,*N*-Dimethylanilines by a Non-Heme Iron(IV)-Oxo Complex

Jiyun Park,[†] Yuma Morimoto,[‡] Yong-Min Lee,[†] Youngmin You,[†] Wonwoo Nam,*[,†] and Shunichi Fukuzumi*[,†,‡]

[†]Department of Bioinspired Science, Ewha Womans University, Seoul 120-750, Korea

[‡]Department of Material and Life Science, Graduate School of Engineering, Osaka University, ALCA, Japan Science and Technology Agency (JST), Suita, Osaka 565-0871, Japan

Supporting Information

ABSTRACT: Oxidative dimerization of *N*,*N*-dimethylaniline (DMA) occurs with a nonheme iron(IV)-oxo complex, $[Fe^{IV}(O)(N4Py)]^{2+}$ (N4Py = *N*,*N*-bis(2-pyridylmethyl)-*N*-bis-(2-pyridyl)methylamine), to yield the corresponding dimer, tetramethylbenzidine (TMB), in acetonitrile. The rate of the oxidative dimerization of DMA by $[Fe^{IV}(O)(N4Py)]^{2+}$ is markedly enhanced by the presence of scandium triflate, $Sc(OTf)_3$ ($OTf = CF_3SO_3^-$), when TMB is further oxidized to the radical cation ($TMB^{\bullet+}$). In contrast, we have observed the oxidative N-demethylation with *para*-substituted DMA substrates, since the position of the C−C bond formation to yield the dimer is blocked. The rate of the oxidative N-demethylation of *para*-substituted DMA by $[Fe^{IV}(O)(N4Py)]^{2+}$ is also markedly enhanced by the presence of $Sc(OTf)_3$. In the case of *para*-substituted DMA derivatives with electron-donating substituents, radical cations of DMA derivatives are initially formed by Sc^{3+} ion-coupled electron transfer from DMA derivatives to $[Fe^{IV}(O)(N4Py)]^{2+}$, giving demethylated products. Binding of Sc^{3+} to $[Fe^{IV}(O)(N4Py)]^{2+}$ enhances the Sc^{3+} ion-coupled electron transfer from DMA derivatives to $[Fe^{IV}(O)(N4Py)]^{2+}$, whereas binding of Sc^{3+} to DMA derivatives retards the electron-transfer reaction. The complicated kinetics of the Sc^{3+} ion-coupled electron transfer from DMA derivatives to $[Fe^{IV}(O)(N4Py)]^{2+}$ are analyzed by competition between binding of Sc^{3+} to DMA derivatives and to $[Fe^{IV}(O)(N4Py)]^{2+}$. The binding constants of Sc^{3+} to DMA derivatives increase with the increase of the electron-donating ability of the *para*-substituent. The rate constants of Sc^{3+} ion-coupled electron transfer from DMA derivatives to $[Fe^{IV}(O)(N4Py)]^{2+}$, which are estimated from the binding constants of Sc^{3+} to DMA derivatives, agree well with those predicted from the driving force dependence of the rate constants of Sc^{3+} ion-coupled electron transfer from one-electron reductants to $[Fe^{IV}(O)(N4Py)]^{2+}$. Thus, oxidative dimerization of DMA and N-demethylation of *para*-substituted DMA derivatives proceed via Sc^{3+} ion-coupled electron transfer from DMA derivatives to $[Fe^{IV}(O)(N4Py)]^{2+}$.

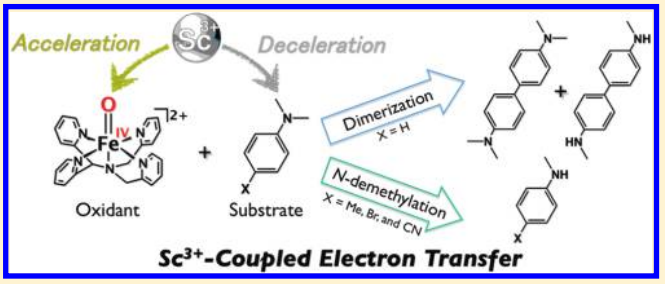

INTRODUCTION

High-valent iron-oxo complexes of heme and nonheme ligands play key roles as reactive intermediates in biological and chemical oxidation reactions.[1,2] The reactivities of the iron-oxo complexes have been extensively investigated over the past several decades, and it has been demonstrated that the reactivities can be controlled by many factors, such as the oxidation state of iron centers and ligand structures.[1,2] In addition, the reactivities of synthetic nonheme iron(IV)-oxo complexes have been intensively investigated in various oxidation reactions,[3] since the first crystal structure of a mononuclear nonheme iron(IV)-oxo complex was reported in 2003.[4] The factors affecting the formation and reactivities of nonheme iron(IV)-oxo complexes in the C−H bond activation and oxo transfer reactions have also been discussed in detail (e.g., supporting and axial ligands and solvents).[5] The reactivities of metal-oxo complexes in the oxidation reactions of alkanes and oxygen atom transfer reactions are controlled not only by the oxidation state of the metal and the ligands[1−7] but also by metal ions acting as Lewis acids.[8] We have shown that the reactivities of the nonheme iron-oxo complexes are markedly affected by the binding of redox inactive metal ions at the iron-oxo centers.[9−11] For example, a crystal structure of Sc^{3+}-bound $[Fe^{IV}(O)(TMC)]^{2+}$ (TMC = 1,4,8,11-tetramethyl-1,4,8,11-tetra-azacyclotetradecane) was determined by X-ray crystallography.[9] In the study, binding of Sc^{3+} to $[Fe^{IV}(O)(TMC)]^{2+}$ has been shown to change the number of electrons transferred from one-electron reductants (e.g., ferrocene) to $[Fe^{IV}(O)(TMC)]^{2+}$.[9] More recently, it has been demonstrated that rates of electron transfer from one-electron reductants to a nonheme iron(IV)-oxo complex,

Received: July 19, 2011
Published: October 19, 2011

$[Fe^{IV}(O)(N4Py)]^{2+}$ (N4Py = *N*,*N*-bis(2-pyridylmethyl)-*N*-bis-(2-pyridyl)methylamine), are enhanced as much as 10^8-fold by addition of Sc^{3+} ion.[10] Such an enhancement of the oxidizing power of nonheme iron(IV)-oxo complexes by metal ions results from strong binding of metal ions to the electron acceptors, which causes large positive shifts in the one-electron reduction potentials, as observed in metal ion-coupled electron-transfer reduction of various electron acceptors.[9−18] On the other hand, binding of metal ions to electron donors results in retardation of electron-transfer reactions of electron donors, because the one-electron oxidation potentials of electron donors are positively shifted by binding of metal ions that results in decreasing the driving force of electron transfer.[19] Thus, there are two opposite effects of metal ion binding on electron transfer: One is acceleration of electron transfer by binding of metal ions to electron acceptors (e.g., metal-oxo complex) and the other is deceleration of electron transfer by binding of metal ions to electron donors (e.g., substrate).[20] However, to the best of our knowledge, there has been no report on such competing effects of redox-inactive metal ions on the oxidation of substrates by metal-oxo complexes.

We report herein that competition between binding of Sc^{3+} ion to *N*,*N*-dimethylaniline (DMA) and $[Fe^{IV}(O)(N4Py)]^{2+}$ results in overall enhancement of electron transfer from DMA to a nonheme iron(IV)-oxo complex, $[Fe^{IV}(O)(N4Py)]^{2+}$. The present study also provides the definitive evidence for the occurrence of electron transfer from DMA to high-valent metal-oxo complexes, although there have been extensive studies on the mechanism of the oxidation of DMA by various oxidants including a possible electron-transfer pathway.[21−28] The complicated kinetics caused by competitive binding of Sc^{3+} ion to DMA and $[Fe^{IV}(O)(N4Py)]^{2+}$ are analyzed as well. While we have observed the formation of a radical cation of DMA dimer, tetramethylbenzidine ($TMB^{\bullet+}$), in the oxidation of DMA by the $[Fe^{IV}(O)(N4Py)]^{2+}$ complex when the reaction is performed in the presence of Sc^{3+} ion, the oxidative N-demethylation reaction takes place with *para*-substituted DMA derivatives, and the oxidative N-demethylation is accelerated by the presence of Sc^{3+} ion. The rate constants of oxidative dimerization and N-demethylation of DMA and its derivatives by $[Fe^{IV}(O)(N4Py)]^{2+}$ in the presence of Sc^{3+} ion are compared with the driving force dependence of Sc^{3+} ion-coupled electron transfer from one-electron reductants to $[Fe^{IV}(O)(N4Py)]^{2+}$ to clarify the oxidation mechanism of DMA derivatives by $[Fe^{IV}(O)(N4Py)]^{2+}$. The extensive analysis on competing effects of binding of Sc^{3+} ion to DMA and its derivatives and to $[Fe^{IV}(O)(N4Py)]^{2+}$ will expand the scope of metal ion-coupled electron transfer on the oxidation of a variety of substrates by high-valent metal-oxo complexes.

EXPERIMENTAL SECTION

Materials. All chemicals were purchased from Sigma-Aldrich, Wako, Nacalai Tesque, and Lancaster Co., Ltd. and used without further purification unless otherwise noted. $[Fe^{II}(N4Py)(MeCN)](ClO_4)_2$ was prepared in a glovebox according to the literature method.[29] Acetonitrile (MeCN) and ether were dried according to the literature procedures and distilled under Ar prior to use.[30] Iodosylbenzene (PhIO) was prepared by a literature method.[31] $[Fe^{IV}(O)(N4Py)]^{2+}$ was prepared by the literature method.[29] Deuterated *N*,*N*-dimethylaniline (DMA-d_6) was prepared by alkylating aniline with CD_3I.[22a] The purities of the compounds were checked by ^1H NMR spectroscopy. Tetra-*n*-butylammonium hexafluorophosphate was purchased from Sigma Chemical Co., recrystallized from ethyl alcohol, and dried under vacuum at 40 °C for at least 1 week prior to use.

Caution! *Perchlorate salts are potentially explosive and should be handled with care.*

General Reaction Procedures. Typically, DMA (4.0×10^{-3} M) was added to a CD_3CN solution (0.50 mL) containing $[Fe^{IV}(O)(N4Py)]^{2+}$ (4.0×10^{-3} M) in the absence and presence of $Sc(OTf)_3$ in an NMR tube. The reaction was complete within 10 min under these conditions. The products in the absence and presence of $Sc(OTf)_3$ were identified as TMB and $[Fe^{II}(N4Py)]^{2+}$ by comparing the ^1H NMR spectra with those of authentic samples. In the case of *para*-substituted DMA derivatives, the demethylated products were formed in the absence and presence of $Sc(OTf)_3$, and they were identified and quantified by comparing the ^1H NMR spectra with those of authentic samples.

Spectral and Kinetic Measurements. Reactions of DMA and its derivatives with $[Fe^{IV}(O)(N4Py)]^{2+}$ (5.0×10^{-5} M) were examined by monitoring spectral changes in the presence of various concentrations of DMA or its derivatives (1.0×10^{-3}−5.0×10^{-2} M) in the absence and presence of $Sc(OTf)_3$ in MeCN at 298 K, with a Hewlett-Packard 8453 photodiode-array spectrophotometer and a quartz cuvette (path length = 10 mm). Kinetic measurements were performed on a UNISOKU RSP-601 stopped-flow spectrometer equipped with a MOS-type highly sensitive photodiode array or a Hewlett-Packard 8453 photodiode-array spectrophotometer at 298 K. Rates of reactions of DMA and its derivatives with $[Fe^{IV}(O)(N4Py)]^{2+}$ were monitored by the decrease of the absorption band due to $[Fe^{IV}(O)(N4Py)]^{2+}$ (λ_{max} = 695 nm) in the absence and presence of $Sc(OTf)_3$ in MeCN. When TMB radical cation ($TMB^{\bullet+}$) was formed in the reaction of DMA with $[Fe^{IV}(O)(N4Py)]^{2+}$ in the presence of $Sc(OTf)_3$ in MeCN, the rate was determined from the increase in the NIR absorption band (λ_{max} = 900 nm) due to $TMB^{\bullet+}$.[32] The concentration of DMA or its derivative was maintained at least more than 10-fold excess of the other reactant to attain pseudo-first-order conditions. Pseudo-first-order rate constants were determined by a least-squares curve fit. The first-order plots were linear for three or more half-lives with the correlation coefficient $\rho > 0.999$. In each case, it was confirmed that the rate constants derived from at least five independent measurements agreed within an experimental error of ±5%.

Electrochemical Measurement. Measurements of cyclic voltammetry (CV) were performed at 298 K using a BAS 630B electrochemical analyzer in a deaerated solvent containing 0.10 M TBAP as a supporting electrolyte at 298 K. A conventional three-electrode cell was used with a platinum working electrode and a platinum wire as a counter electrode. The measured potentials were recorded with respect to the $Ag/AgNO_3$ (1.0×10^{-2} M). The E_{ox} and E_{red} values (vs $Ag/AgNO_3$) are converted to those versus SCE by adding 0.29 V.[33] All electrochemical measurements were carried out under an Ar atmosphere.

EPR Measurements. Electron paramagnetic resonance (EPR) detection of $TMB^{\bullet+}$ was performed as follows: Typically, a MeCN solution of $[Fe^{IV}(O)(N4Py)]^{2+}$ (3.0×10^{-4} M) in the presence of $Sc(OTf)_3$ (3.0×10^{-4} M) in an EPR cell (3.0 mm i.d.) was purged with Ar for 5 min. Then, DMA (8.0×10^{-4} M) was added to the solution. The EPR spectrum of $TMB^{\bullet+}$ was recorded on a JEOL JES-RE1XE spectrometer at 243 K. The magnitude of modulation was chosen to optimize the resolution and signal-to-noise (S/N) ratio of the observed spectra under nonsaturating microwave power conditions. The *g* value was calibrated using a Mn^{2+} marker (g = 2.034, 1.981). Computer simulation of the EPR spectra was carried out by using Calleo EPR version 1.2 (Calleo Scientific Publisher) on a personal computer.

RESULTS AND DISCUSSION

Three-Electron Oxidation of DMA by $[Fe^{IV}(O)(N4Py)]^{2+}$ in the Presence of Sc^{3+}. DMA has been suggested to be oxidized by nonheme iron(IV)-oxo complexes such as $[Fe^{IV}(O)(N4Py)]^{2+}$ to

Scheme 1

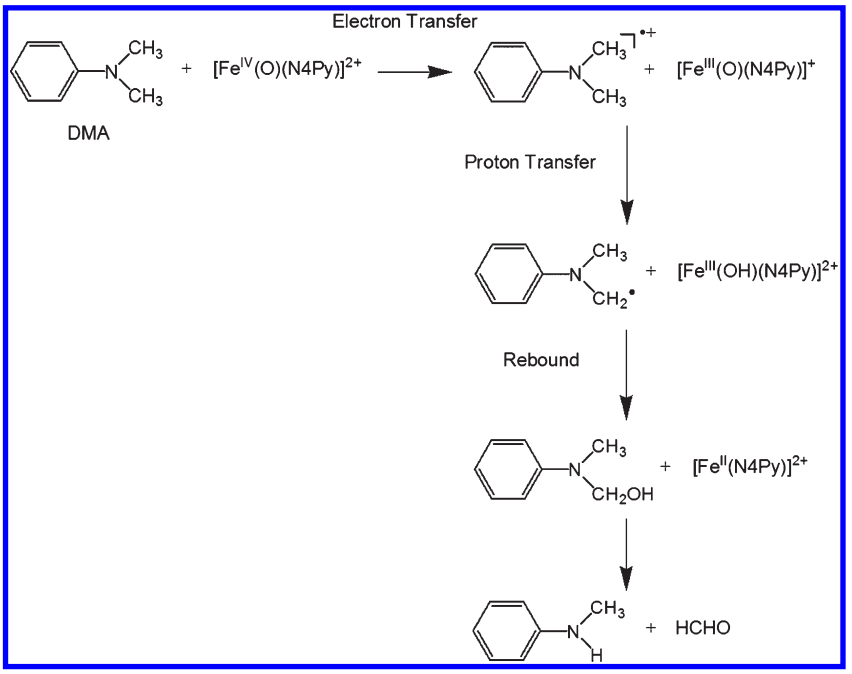

yield the demethylated product (*N*-methylaniline) via an electron transfer-proton transfer (ET-PT) mechanism,[27] as shown in Scheme 1. Electron transfer from DMA to $[Fe^{IV}(O)(N4Py)]^{2+}$ is followed by proton transfer from $DMA^{\bullet+}$ and $[Fe^{III}(O)(N4Py)]^{+}$ to yield the DMA radical and $[Fe^{III}(OH)(N4Py)]^{2+}$, because $DMA^{\bullet+}$ and $[Fe^{III}(O)(N4Py)]^{+}$ are a strong acid and base, respectively. The rebound between DMA radical and $[Fe^{III}(OH)(N4Py)]^{2+}$ results in formation of the demethylated product. However, the intermediate $DMA^{\bullet+}$ formed in the ET-PT mechanism cannot be detected because the initial ET process is the rate-determining step.[27]

In the presence of $Sc(OTf)_3$, however, the oxidized product of DMA by $[Fe^{IV}(O)(N4Py)]^{2+}$ was changed from the demethylated product in the absence of $Sc(OTf)_3$ to the dimer radical cation, that is, tetramethylbenzidine radical cation ($TMB^{\bullet+}$). The quantitative formation of $TMB^{\bullet+}$ in the reaction of DMA with $[Fe^{IV}(O)(N4Py)]^{2+}$ in the presence of $Sc(OTf)_3$ in MeCN is shown in Figure 1a, where the absorption bands at 470, 900, and 1000 nm are assigned due to $TMB^{\bullet+}$.[32,34] The same absorption bands due to $TMB^{\bullet+}$ are observed in the one-electron oxidation of TMB by a strong one-electron oxidant $[Ru(bpy)_3]^{3+}$ and cerium(IV) ammonium nitrate (Figure 1b and 1c). The $TMB^{\bullet+}$ produced by the one-electron oxidation of TMB by 1 equiv of $[Ru(bpy)_3]^{3+}$ was oxidized to TMB^{2+} by further addition of $[Ru(bpy)_3]^{3+}$ as shown in Figure 1b (right panel), because the second one-electron oxidation potential of TMB (0.68 V vs SCE)[35] is still lower than the one-electron reduction potential of $[Ru(bpy)_3]^{3+}$ (1.24 V vs SCE). The concentration of $TMB^{\bullet+}$ was determined using the ε value at 900 nm [$2.0 \times 10^4\ M^{-1}\ cm^{-1}$; see Figure 1b, right panel] to be 1.0×10^{-4} M, which is one-third of the initial concentration of $[Fe^{IV}(O)(N4Py)]^{2+}$ (3.0×10^{-4} M). Thus, three-electron oxidation of DMA occurs with $[Fe^{IV}(O)(N4Py)]^{2+}$ to yield $TMB^{\bullet+}$. The formation of $TMB^{\bullet+}$ was also confirmed by the EPR spectrum (Supporting Information, Figure S1).[36]

The drastic change of the oxidized product of DMA with $[Fe^{IV}(O)(N4Py)]^{2+}$ upon addition of $Sc(OTf)_3$ is well understood as shown in Scheme 2, which is in line with Scheme 1. The initial electron transfer from DMA to $[Fe^{IV}(O)(N4Py)]^{2+}$ is much enhanced by Sc^{3+} ion, as observed in Sc^{3+} ion-coupled electron transfer from one-electron reductants to $[Fe^{IV}(O)(N4Py)]^{2+}$, to yield $DMA^{\bullet+}$ and the Sc^{3+} ion-bound Fe(III)-oxo complex. The proton transfer from $DMA^{\bullet+}$ to the Fe(III)-oxo complex may be prohibited by the strong binding of Sc^{3+} to the Fe(III)-oxo complex. In such a case, $DMA^{\bullet+}$ undergoes the dimerization to produce TMB, via the reaction with DMA that acts as a nucleophile, accompanied by the oxidation and removal of two protons (Scheme 2).[32] Judging from the significantly lower one-electron oxidation potential of TMB (E_{ox} = 0.43 V vs SCE)[37] as compared with DMA (E_{ox} = 0.76 V vs SCE),[38] TMB is further oxidized by $[Fe^{IV}(O)(N4Py)]^{2+}$ (E_{red} = 0.51 V vs SCE)[10] to produce $TMB^{\bullet+}$. The formation of $TMB^{\bullet+}$ by the one-electron oxidation of TMB by $[Fe^{IV}(O)(N4Py)]^{2+}$ in the presence of Sc^{3+} was confirmed as shown in the Supporting Information, Figure S2. Thus, Sc^{3+} ion-coupled electron transfer from DMA to $[Fe^{IV}(O)(N4Py)]^{2+}$ results in the three-electron oxidation of DMA by $[Fe^{IV}(O)(N4Py)]^{2+}$ to yield $TMB^{\bullet+}$ rather than the demethylated product in the presence of Sc^{3+}. At prolonged reaction time, deprotonation of $TMB^{\bullet+}$ occurs slowly to yield the demethylated product of TMB, *N*,*N*-dimethylbenzidine (DMB), together with the Fe(II) complex (Supporting Information, Figures S3 and S4).[39] The right panel of Figure 1c indicates the rapid formation of $DMA^{\bullet+}$ (rise in absorbance at 900 nm) and the subsequent slow conversion to $TMB^{\bullet+}$ (decay in absorbance at 470 nm).

According to Scheme 2, once Sc^{3+} ion-coupled electron transfer from DMA to $[Fe^{IV}(O)(N4Py)]^{2+}$ occurs, protons are produced in the radical coupling reaction of $DMA^{\bullet+}$ to yield TMB. In such a case, proton-coupled electron transfer from DMA to $[Fe^{IV}(O)(N4Py)]^{2+}$ may occur, leading to formation of

dx.doi.org/10.1021/ic201545a |*Inorg. Chem.* 2011, 50, 11612–11622

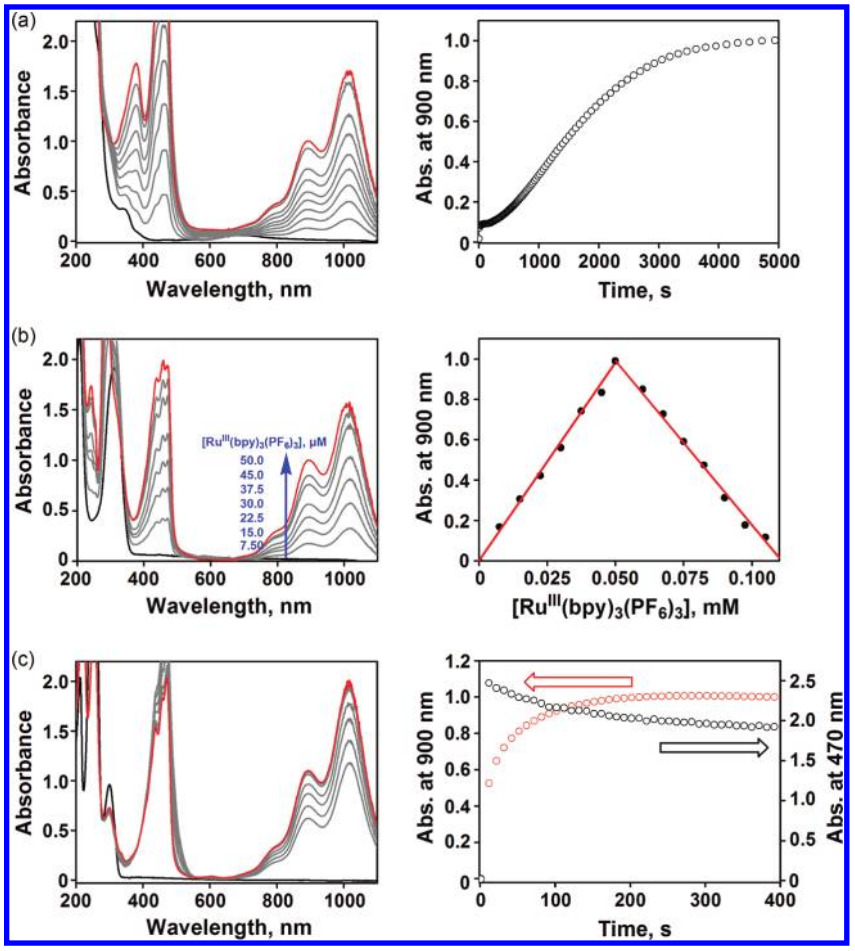

Figure 1. (a) Visible spectral changes observed in the reaction of $[Fe^{IV}(O)(N4Py)]^{2+}$ (0.15 mM) with DMA (0.44 mM) in the presence of $Sc(OTf)_3$ (0.15 mM) in MeCN at 298 K (left panel). Right panel shows time course monitored at 900 nm. (b) Visible spectral changes observed in the formation of $TMB^{\bullet+}$ by titration of TMB (0.050 mM) with $[Ru(bpy)_3](ClO_4)_3$ (0−0.050 mM) in MeCN at 298 K (left panel). Right panel shows Job's plot of absorbance changes monitored at 900 nm due to $TMB^{\bullet+}$ upon addition of $[Ru^{III}(bpy)_3](PF_6)_3$ (0−0.105 mM) into the solution of TMB (0.050 mM) in MeCN at 298 K. (c) Visible spectral changes observed in the reaction of DMA (0.30 mM) with cerium(IV) ammonium nitrate (0.20 mM) in MeCN at 298 K (left panel). Right panel shows time courses monitored at 470 and 900 nm.

$TMB^{\bullet+}$ as shown in Scheme 3. The $TMB^{\bullet+}$ concentration formed in the reaction of DMA with $[Fe^{IV}(O)(N4Py)]^{2+}$ was confirmed by the titration of Sc^{3+} concentration as shown in Figure 2. Only a catalytic amount of $Sc(OTf)_3$ (e.g., 1/9 of $[Fe^{IV}(O)(N4Py)]^{2+}$) is enough to obtain the stoichiometric amount of $TMB^{\bullet+}$ (Supporting Information, Figure S5).[40] The careful re-examination of the products of the reaction of DMA with $[Fe^{IV}(O)(N4Py)]^{2+}$ in the absence of $Sc(OTf)_3$ revealed formation of DMB, demethylated product of TMB, (9% based on the initial concentration of $[Fe^{IV}(O)(N4Py)]^{2+}$) as well as *N*-methylaniline (62%) and TMB (1%) as the final products (Supporting Information, Figure S6). Because DMB and TMB are the six-electron and two-electron oxidized products of DMA, respectively, the overall yield based on $[(N4Py)Fe^{IV}(O)]^{2+}$ (a two-electron oxidant) will be 9 × 3 + 1 + 62 = 90%. Thus, even in the absence of $Sc(OTf)_3$, the dimerization of $DMA^{\bullet+}$ competes with proton transfer from $DMA^{\bullet+}$ to the Fe(III)-oxo complex.

Sc^{3+}-Enhanced Demethylation of X-DMA with $[Fe^{IV}(O)(N4Py)]^{2+}$. When DMA is replaced by *para*-cyano-*N*,*N*-dimethylaniline (CN-DMA), no dimer radical cation was formed even in the presence of $Sc(OTf)_3$, because the *para*-position is blocked by the CN group and the demethylated product was obtained predominantly as identified by the ^1H NMR spectrum (Supporting Information, Figures S7 and S8). The absorption spectral change in the reaction of CN-DMA with $[Fe^{IV}(O)(N4Py)]^{2+}$ in the absence and the presence of $Sc(OTf)_3$ in MeCN is shown in Figures 3a and 3b, respectively. In the presence of $Sc(OTf)_3$, the reaction rate was much enhanced as compared with that in the absence of $Sc(OTf)_3$ and therefore the spectra in Figure 3b were measured using a stopped-flow spectrophotometer.[41] $Sc(OTf)_3$ is known to exist as a free ion (Sc^{3+}) in solution.[10] In each case only the decay of absorbance at 695 nm due to $[Fe^{IV}(O)(N4Py)]^{2+}$ was observed (i.e., no formation of dimer radical cation was observed). The decay rate of $[Fe^{IV}(O)(N4Py)]^{2+}$ with large excess CN-DMA and Sc^{3+} obeyed first-order kinetics (see Supporting Information, Table S1). Under the conditions in Figure 1a, the reaction was slowed down because of the small concentration of DMA (0.44 mM) and $Sc(OTf)_3$ (0.15 mM). In such a case the proton-coupled electron transfer in Scheme 3 plays a major role as the reaction proceed. This may be the reason why an induction period is observed in Figure 1a (right panel). To avoid the contribution of the proton-coupled electron transfer, the kinetic measurements were performed using a

dx.doi.org/10.1021/ic201545a |*Inorg. Chem.* 2011, 50, 11612–11622

Scheme 2

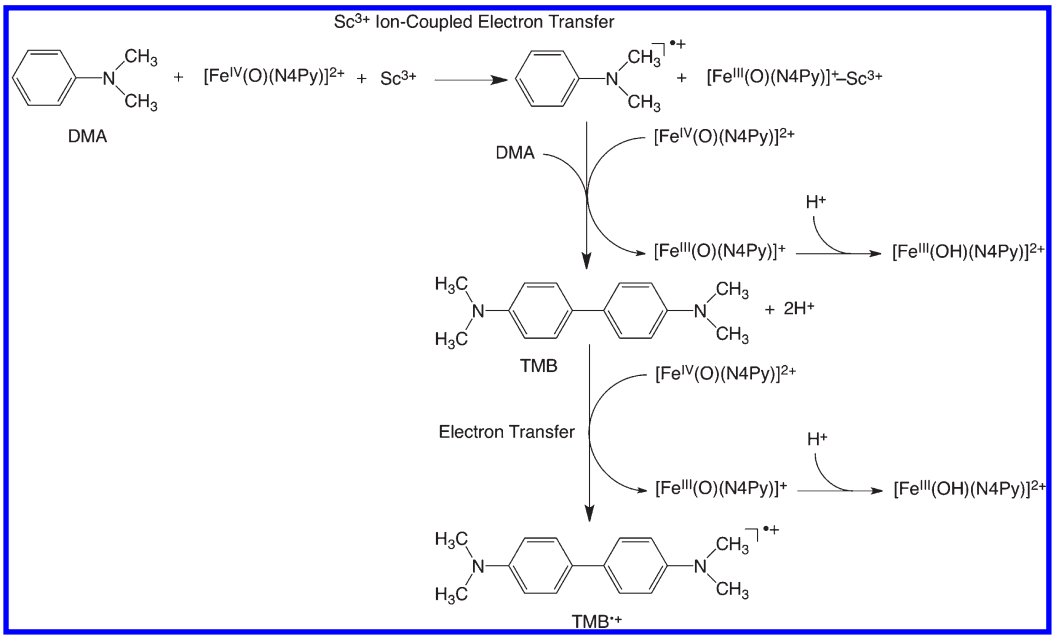

Scheme 3

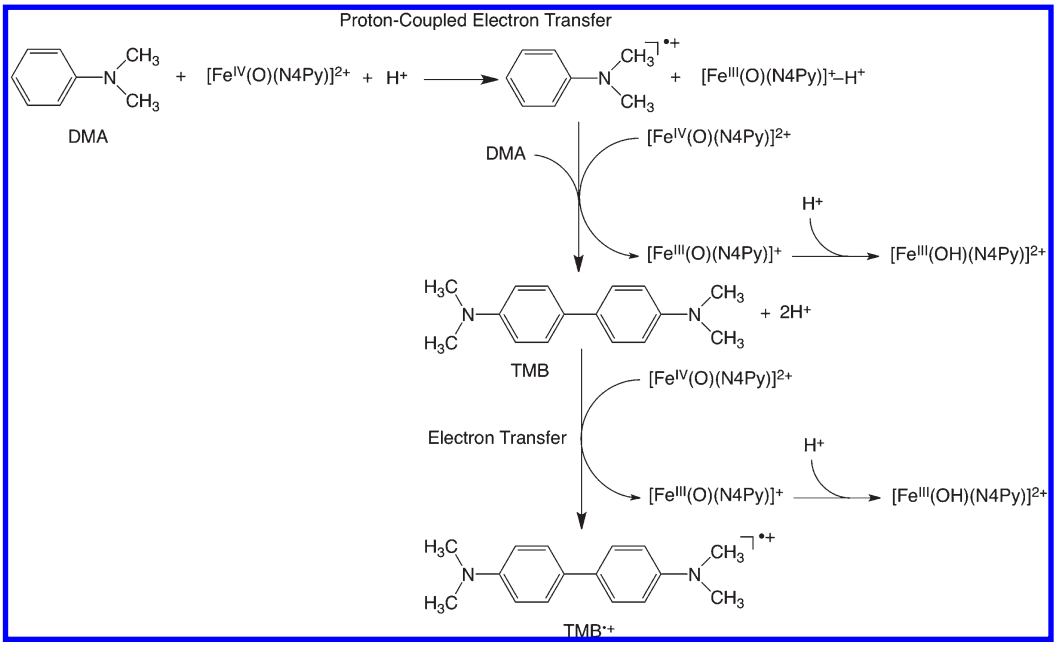

large concentration of Sc^{3+} (e.g., 10 mM). For the kinetic measurements no induction period was observed as shown in Figure 3b.

The observed first-order rate constant (k_{obs}) in the presence of $Sc(OTf)_3$ becomes much larger than that in the absence of $Sc(OTf)_3$. Similar results are obtained for other *para*-substituted DMA derivatives (see Supporting Information, Figure S9).

Figure 4 shows the dependence of k_{obs} on concentration of $Sc(OTf)_3$. The k_{obs} values increase linearly with increasing Sc^{3+} concentration in the region where Sc^{3+} concentrations are larger than the concentration of DMA derivatives (X-DMA). Plots of k_{obs} versus [Sc(OTf)] − [X-DMA] afford linear correlations (Figure 4, right panels). This indicates that Sc^{3+} forms a 1:1 complex with X-DMA and that Sc^{3+}-bound X-DMA is inert toward oxidation.

On the other hand, the k_{obs} value increases with increasing concentration of CN-DMA to reach a constant value in the region where concentrations of CN-DMA are larger than Sc^{3+} concentration as shown in Figure 5. This also indicates that Sc^{3+} binds with CN-DMA to form a 1:1 complex, and the acceleration

dx.doi.org/10.1021/ic201545a |*Inorg. Chem.* 2011, 50, 11612–11622

of the rate requires Sc^{3+} ion, which is not bound to CN-DMA. Similar results were obtained for other *para*-substituted DMA (X-DMA). Thus, the enhanced reactivity of X-DMA observed in the presence of Sc^{3+} is ascribed to Sc^{3+} ion-coupled electron transfer from X-DMA to $[Fe^{IV}(O)(N4Py)]^{2+}$, as shown in Scheme 4.

Because Sc^{3+} ions bound to X-DMA and $[Fe^{IV}(O)(N4Py)]^{2+}$ are in equilibrium with free Sc^{3+} ions in Scheme 4, there may be exchange equilibria among them.

Electron transfer from X-DMA to $[Fe^{IV}(O)(N4Py)]^{2+}$ is enhanced by binding of Sc^{3+} to $[Fe^{IV}(O)(N4Py)]^{2+}$, which competes with the binding of Sc^{3+} to X-DMA. It has been reported that one Sc^{3+} ion or two Sc^{3+} ions can bind to $[Fe^{IV}(O)(N4Py)]^{2+}$ to enhance the electron-transfer reduction of $[Fe^{IV}(O)(N4Py)]^{2+}$.[10] In the case of DMA, the dimerization of $DMA^{\bullet+}$ may occur much more rapidly than proton transfer from $DMA^{\bullet+}$ to the Sc^{3+} ion-bound Fe(III)-oxo complex (Scheme 2). In the case of X-DMA, however, the dimerization of $X\text{-}DMA^{\bullet+}$ is prohibited by the *para*-substituent and proton transfer from $X\text{-}DMA^{\bullet+}$ to the Sc^{3+} ion-bound Fe(III)-oxo complex occurs that leads to the formation of the demethylated product, as shown in Scheme 1.

The results in Figure 4 and Figure 5 can be explained by Scheme 4. It should be emphasized that only uncomplexed Sc^{3+} and DMA are involved in Sc^{3+}ion-coupled electron transfer in Scheme 4, where two Sc^{3+} ions are involved as reported previously.[10] Under the conditions ($[Sc^{3+}]$ > [X-DMA]) in Figure 4, Sc^{3+} ion-coupled electron transfer from free X-DMA to free Sc^{3+} is accelerated showing the second-order dependence on $[Sc^{3+}]$. At a constant concentration of X-DMA (5 mM), the concentration of free DMA decreases with increasing $[Sc^{3+}]$. For example, by using the K_0 value (620 M^{-1}), the ratio of free DMA concentration to the total concentration (5 mM) at 20 mM Sc^{3+} is only 9.1%. Thus, the concentration of free DMA is inversely proportional to concentration of Sc^{3+}: $[Sc^{3+}]^{-1}$. The second-order acceleration of the rate $[Sc^{3+}]^2$ is canceled by the dependence of the ratio of free DMA on $[Sc^{3+}]^{-1}$. As a result, we can observe the apparent linear acceleration of the first-order rate constant with increasing concentration of Sc^{3+} in the region where $[Sc^{3+}]$ > [DMA] in Figure 4. On the other hand, under the conditions ($[Sc^{3+}]$ = 50 mM) in Figure 5, the first-order rate constant increases with increasing concentration of DMA, but reaches a constant value in the region where [X-DMA] > $[Sc^{3+}]$, because the concentration of free Sc^{3+} is inversely proportional to concentration of DMA: $[DMA]^{-1}$. As a result, the first-order dependence of the rate on [X-DMA] is canceled by the dependence of the concentration of free Sc^{3+} on $[X\text{-}DMA]^{-1}$ to be a constant value in the region where [X-DMA] > $[Sc^{3+}]$ in Figure 5. More quantitative analysis in Figure 4 is given below.

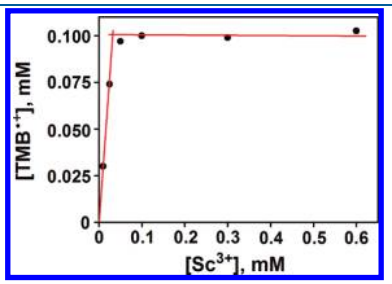

Figure 2. Plot of concentration of $TMB^{\bullet+}$ produced in the reaction of $[Fe^{IV}(O)(N4Py)]^{2+}$(0.30 mM) with DMA (0.6−1.4 mM) in the presence of Sc^{3+} in MeCN at 298 K vs Sc^{3+} concentration.

According to Scheme 4, the reaction rate ($-d[Fe^{IV}(O)]/dt$ where $[Fe^{IV}(O)] = [[Fe^{IV}(O)(N4Py)]^{2+}]$) is given by eqs 1 and 2,

$$-d[Fe^{IV}(O)]/dt = k_{et}[Fe^{IV}(O)][X\text{-}DMA] \quad (1)$$

$$k_{et} = (k_{et0} + k_{et1}K_1[Sc^{3+}] + k_{et2}K_1K_2[Sc^{3+}]^2) \quad (2)$$

where k_{et0}, k_{et1}, and k_{et2} are the rate constants of electron transfer from X-DMA to $[Fe^{IV}(O)(N4Py)]^{2+}$, $[Fe^{IV}(O)(N4Py)]^{2+}-Sc^{3+}$, and $[Fe^{IV}(O)(N4Py)]^{2+}-(Sc^{3+})_2$, respectively. K_1 and K_2 are the binding constants of Sc^{3+} to $[Fe^{IV}(O)(N4Py)]^{2+}$ and $[Fe^{IV}(O)(N4Py)]^{2+}-Sc^{3+}$, respectively. On the other hand, the concentration of Sc^{3+}-bound X-DMA $[X\text{-}DMA-Sc^{3+}]$ is given by eq 3,

$$[X\text{-}DMA\text{-}Sc^{3+}] = K_0[X\text{-}DMA][Sc^{3+}] \quad (3)$$

where K_0 is the binding constant of Sc^{3+} to X-DMA.

When $[Sc^{3+}]_0 \ll [X\text{-}DMA]_0$ and $1 \ll K_0[DMA]$ (the subscript 0 denotes the initial concentration), $[X\text{-}DMA] \cong [X\text{-}DMA]_0$, $[Sc^{3+}] \cong [Sc^{3+}]_0/K_0[X\text{-}DMA]_0$. In such a case, the binding of Sc^{3+} to $[Fe^{IV}(O)(N4Py)]^{2+}-Sc^{3+}$ may be negligible because of the small concentration of free Sc^{3+}, and the observed first-order rate constant (k_{obs}) is given from eqs 1−3 by eq 4, where k_{et0} is neglected. This equation agrees with the constant dependence of k_{obs} on [X-DMA] in the region where $[Sc^{3+}] \ll$ [X-DMA] in Figure 5.

$$k_{obs} \cong k_{et1}K_1[Sc^{3+}]_0/K_0 \quad (4)$$

When $[Sc^{3+}] \gg$ [X-DMA] and $K_0[Sc^{3+}] \gg 1$, $[Sc^{3+}] \cong [Sc^{3+}]_0$, $[X\text{-}DMA] \cong [X\text{-}DMA]_0/K_0[Sc^{3+}]_0$. In such a case the binding of Sc^{3+} to $[Fe^{IV}(O)(N4Py)]^{2+}-Sc^{3+}$ (K_2) may be dominant as

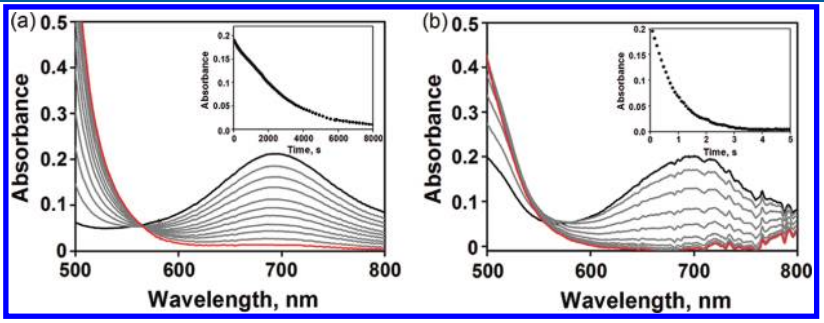

Figure 3. Visible spectral changes observed in the reaction of $[Fe^{IV}(O)(N4Py)]^{2+}$ (0.50 mM) with CN-DMA (5.0 mM) in the absence (a) and presence (b) of Sc^{3+} (15 mM) in MeCN at 298 K. Insets show time courses monitored at 695 nm.

dx.doi.org/10.1021/ic201545a |*Inorg. Chem.* 2011, 50, 11612–11622

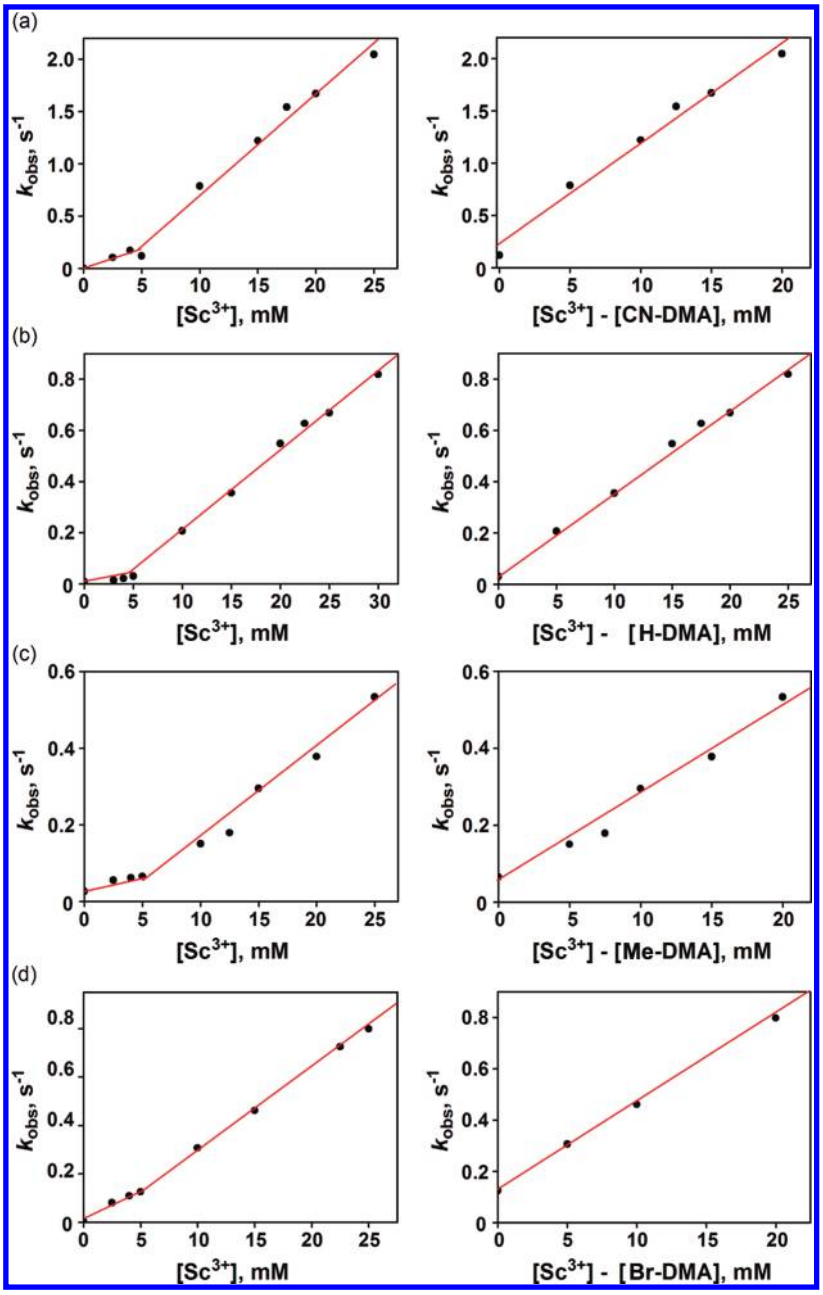

Figure 4. Plots of k_{obs} vs [Sc^{3+}] (left panels) and [Sc^{3+}] − [X-DMA] (right panels) in the reaction of [Fe^{IV}(O)(N4Py)]$^{2+}$ (0.50 mM) and X-DMA (5.0 mM) (X = CN (a), H (b), Me (c), and Br (d)) in the presence of Sc^{3+} in MeCN at 298 K.

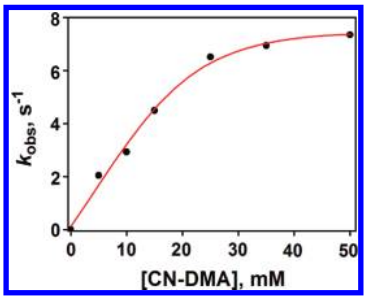

Figure 5. Plot of k_{obs} vs [CN-DNA] in the reaction of [Fe^{IV}(O)(N4Py)]$^{2+}$ (0.50 mM) and CN-DNA in the presence of Sc^{3+} (50 mM) in MeCN at 298 K.

compared to the binding of Sc^{3+} to [Fe^{IV}(O)(N4Py)]$^{2+}$ (K_1) and k_{obs} is given by eq 5, which agrees with the linear dependence of k_{obs} on [Sc^{3+}] in the region where [Sc^{3+}] > [X-DMA] in Figure 4 and also the linear dependence of k_{obs} on [X-DMA] in the region where [X-DMA] ≪ [Sc^{3+}] in Figure 5.

$$k_{obs} \cong k_{et2}K_1K_2[Sc^{3+}]_0[X\text{-}DMA]_0/K_0 \quad (5)$$

The complex formation of X-DMA with Sc^{3+} is also indicated by the UV−vis spectral change of X-DMA in the presence of $Sc(OTf)_3$. As shown in Figure 6, the absorption band at 293 nm due to CN-DMA is changed because of formation of the CN-DMA−Sc^{3+} complex with a clean isosbestic point. The K_0 value

dx.doi.org/10.1021/ic201545a |*Inorg. Chem.* 2011, 50, 11612–11622

Scheme 4

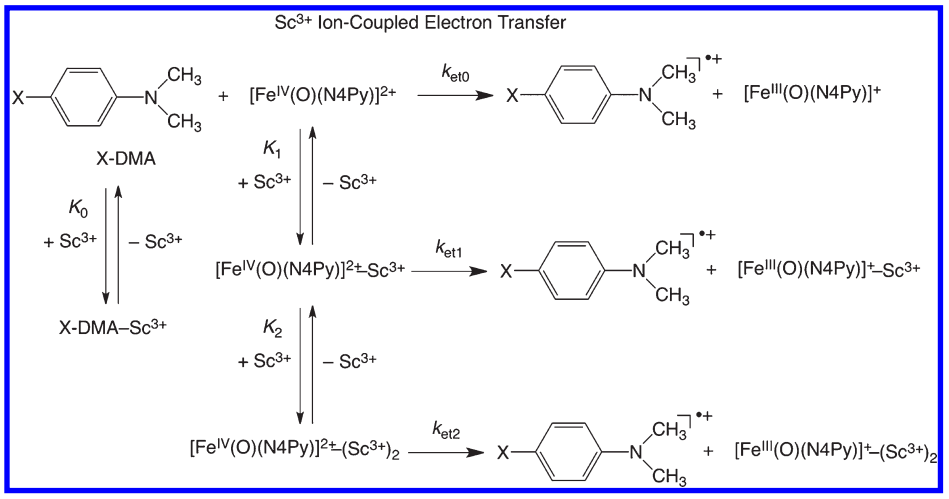

is determined from the intercept and slope of the linear plot of $(\Delta A)^{-1}$ versus $[Sc^{3+}]^{-1}$ (Figure 6c) to be 6.2×10^2 M^{-1}. The UV−vis spectral titrations of other DMA derivatives with Sc^{3+} are shown in Supporting Information, Figure S10. The spectral titration of X-DMA with $Sc(OTf)_3$ indicates that Sc^{3+} forms a 1:1 complex with X-DMA. The 1:1 complex formation between X-DMA and Sc^{3+} was also confirmed by the ^1H NMR spectra (see Supporting Information, Figures S11−S15). The change in the chemical shift of the *N*-Me group by binding of Sc^{3+} indicates that Sc^{3+} ion binds to the nitrogen of the *N*-Me group of X-DMA. The binding constants K_0 were determined from the spectral change of X-DMA with Sc^{3+} and the K_0 values thus determined are listed in Table 1 together with the one-electron oxidation potentials of X-DMA (E_{ox}). The K_0 value increases with decreasing the E_{ox} value. This indicates that the stronger the electron donor ability of X-DMA is, the larger becomes the binding constant of Sc^{3+} to X-DMA.

The k_{obs} values with 5.0 mM X-DMA and 15 mM Sc^{3+} are also listed in Table 1 together with k_{obs} values in the absence of $Sc(OTf)_3$ in MeCN at 298 K. The k_{obs} values in the presence of Sc^{3+} (15 mM) are significantly larger than those in the absence of Sc^{3+} for each X-DMA. In the absence of Sc^{3+}, the k_{obs} value increases with decreasing the E_{ox} value of X-DMA and Me-DMA with an electron-donating *para*-substituent affords the largest k_{obs} value, whereas CN-DMA with an electron-withdrawing substituent affords the largest k_{obs} value in the presence of Sc^{3+}. This results from the binding of Sc^{3+} to X-DMA. As mentioned above, Sc^{3+}-bound DMA derivatives exhibit negligible reactivity as compared with Sc^{3+}−free DMA derivatives.

This was confirmed by the change in the one-electron oxidation potential (E_{ox}) of X-DMA in the presence of $Sc(OTf)_3$ as shown in Figure 7, where the redox couple of CN-DMA in the absence of Sc^{3+} at $E_{1/2}$ = 1.13 V (vs SCE) disappears as the concentration of Sc^{3+} increases. No anodic peak of CN-DMA is observed in the presence of a large excess $Sc(OTf)_3$ (10 mM). This indicates that the E_{ox} value of CN-DMA (1.13 V vs SCE)[36] is positively shifted to the value larger than 2.0 V (vs SCE) when Sc^{3+} is bound to CN-DMA. Thus, once Sc^{3+} is bound to X-DMA, the X-DMA−Sc^{3+} complex cannot act as an electron donor and only free X-DMA is involved in the Sc^{3+} ion-coupled electron transfer to $[Fe^{IV}(O)(N4Py)]^{2+}$ (E_{red} = 1.19 V vs SCE in the presence of 10 mM of Sc^{3+})[10] as shown in Scheme 4.

The second-order rate constant (k_{et}) of Sc^{3+} ion-coupled electron transfer from free X-DMA, which is not bound to Sc^{3+}, to $[Fe^{IV}(O)(N4Py)]^{2+}$ is derived from the observed pseudo-first-order rate constant (k_{obs}) with large excess X-DMA as given by eq 6, because

$$k_{et} \cong k_{obs}(K_0[Sc^{3+}] + 1)/[\text{X-DMA}]_0 \quad (6)$$

$[\text{X-DMA}] = [\text{X-DMA}]_0/(1 + K_0[Sc^{3+}])$ according to eq 3 (note that $[\text{X-DMA}]_0 = [\text{X-DMA}] + [\text{X-DMA}{-}Sc^{3+}]$). The k_{et} values thus evaluated from the k_{obs} values are listed in Table 1, where the concentration of free Sc^{3+}, which is not bound to X-DMA, is 10 mM ($[Sc^{3+}]_0 - [\text{X-DMA}]_0$). For example, the k_{et} value of DMA was determined from the k_{obs} value (0.36 s^{-1} in Table 1) using eq 6 to be 5.3×10^6 M^{-1} s^{-1} ($= 0.36 \times (7.3 \times 10^6 \times 1.0 \times 10^{-2} + 1)/(5.0 \times 10^{-3})$).

Driving Force of Sc^{3+}-Coupled Electron Transfer. The driving force dependence of the rate constants (k_{et0}) of the demethylation reactions of X-DMA with $[Fe^{IV}(O)(N4Py)]^{2+}$ in the absence of Sc^{3+} is shown in Figure 8 together with the driving force dependence of the rate constants (k_{et}) of Sc^{3+} ion-coupled electron transfer from free X-DMA, which is not bound to Sc^{3+}, and various one-electron reductants to $[Fe^{IV}(O)(N4Py)]^{2+}$. The driving force dependence of k_{et} is well fitted in light of the Marcus theory of adiabatic outer-sphere electron transfer (eq 7), where Z is the collision frequency taken as 1×10^{11} M^{-1} s^{-1}, λ is the reorganization energy of electron transfer, k_B is the Boltzmann constant, and T is the absolutetemperature.[43]

$$k_{et} = Z\exp[-(\lambda/4)(1 + \Delta G_{et}/\lambda)^2/k_B T] \quad (7)$$

The best fit λ value of Sc^{3+} ion-coupled electron transfer from X-DMA, which is not bound to Sc^{3+}, to $[Fe^{IV}(O)(N4Py)]^{2+}$ is determined to be 1.79 eV, which is smaller than the λ value of electron transfer from one-electron reductants (2.27 eV).[10] The smaller λ value Sc^{3+} ion-coupled electron transfer from X-DMA to $[Fe^{IV}(O)(N4Py)]^{2+}$ may result from the smaller λ value of electron exchange between X-DMA and X-DMA$^{\bullet+}$ as compared with the λ values of metal complexes used as one-electron

dx.doi.org/10.1021/ic201545a |*Inorg. Chem.* 2011, 50, 11612–11622

reductants. Thus, the demethylation of X-DMA with $[Fe^{IV}(O)(N4Py)]^{2+}$ in the presence of Sc^{3+} proceeds via Sc^{3+} ion-coupled electron transfer from X-DMA to $[Fe^{IV}(O)(N4Py)]^{2+}$ as shown in Scheme 4.

In the absence of Sc^{3+}, the k_{et0} values of Me-DMA and DMA agree with those predicted by the Marcus plot of electron transfer with $\lambda = 2.02$ eV. With increasing the E_{ox} values of X-DMA with electron withdrawing *para*-substituents (Br and CN), the deviation of the observed rate constant from the predicted value by the Marcus plot of electron transfer becomes larger, when the $-\Delta G_{et}$ value becomes more positive than 0.4 eV. Thus, the borderline between a direct hydrogen atom transfer pathway and an electron-transfer pathway (Scheme 1) may be determined by the E_{ox} value of X-DMA, about 1.2 V versus SCE that corresponds to Br-DMA. It is interesting to note that this borderline is virtually the same as reported between oxygen atom transfer pathway and an electron transfer pathway for the oxygenation of thioanisole derivatives with $[Fe^{IV}(O)(N4Py)]^{2+}$ as shown in Figure 8 (no. 5−10).[11]

It is also important to note that through the use of DMA and deuterated DMA (*N*,*N*-dimetyl-d_6-aniline; DMA-d_6) as a substrate in the presence of Sc^{3+}, the k_{obs} values increase linearly with increasing Sc^{3+} concentration in the region where Sc^{3+} concentrations are larger than the concentration of DMA and DMA-d_6, respectively, and no deuterium kinetic isotope effect (KIE) was observed, that is, KIE = 1.0 (see Supporting Information, Figure S16). This result confirms that the initial Sc^{3+} ion-coupled

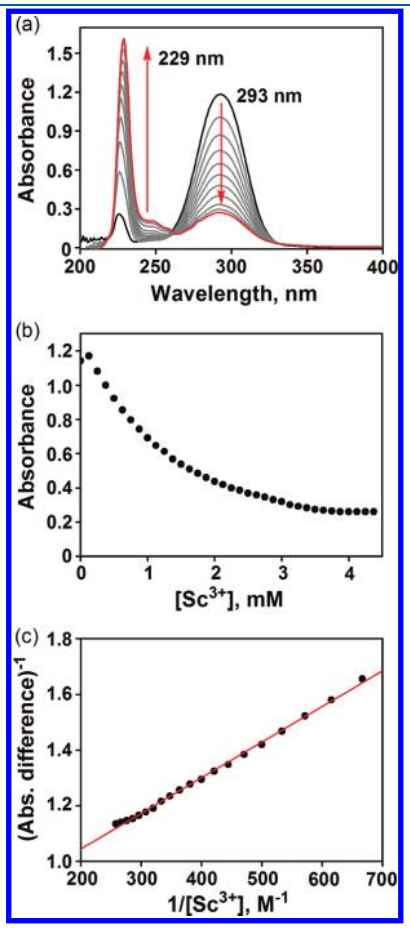

Figure 6. (a) Visible spectral changes observed in the titration of CN-DMA with Sc^{3+} upon addition of Sc^{3+} (0.0−4.0 mM) into the CN-DMA solution (0.050 mM) in MeCN at 298 K. (b) Plot of the absorbance at 293 nm vs $[Sc^{3+}]$ in the titration of CN-DMA with Sc^{3+} upon addition of Sc^{3+} (0.0−4.0 mM) into the CN-DMA solution (0.050 mM) in MeCN at 298 K. (c) Plot of reciprocal absorbance difference vs $1/[Sc^{3+}]$ for the determination of the binding constant between *p*-CN-DMA and Sc^{3+} (see Supporting Information, Figure S10 for the other case of X-DMA).

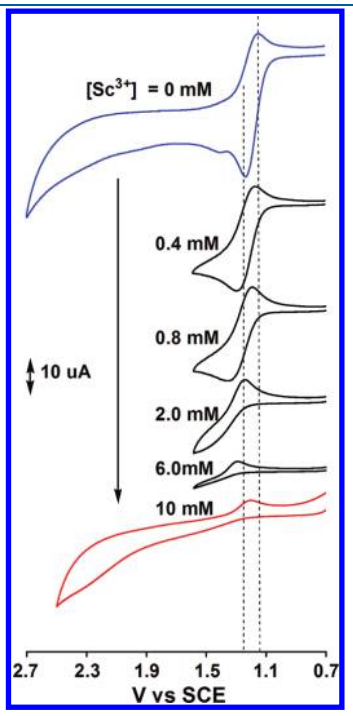

Figure 7. Cyclic voltammograms of CN-DMA (2.0 mM) upon addition of $Sc(OTf)_3$ into an MeCN solution of CN-DMA containing $TBAPF_6$ (0.10 M) at 298 K with a Pt working electrode. Scan rate was 0.10 V s^{-1}.

Table 1. Binding Constants (K_0) of Sc^{3+} with X-DMA, One-Electron Oxidation Potentials (E_{ox} vs SCE) of X-DMA, Rate Constants of Reactions of $[Fe^{IV}(O)(N4Py)]^{2+}$ (0.50 mM) with X-DMA (5.0 mM) in the Absence and Presence of Sc^{3+} (15 mM) in MeCN at 298 K

X	E_{ox} vs SCE, V	K_0[a], M^{-1}	k_{obs}[b], s^{-1}	k_{obs}[c], s^{-1}	k_{et}[d], M^{-1} s^{-1}
Me	0.69	$(3.0 \pm 0.3) \times 10^7$	$(2.6 \pm 0.2) \times 10^{-2}$	$(3.0 \pm 0.2) \times 10^{-1}$	$(1.8 \pm 0.2) \times 10^7$
H	0.76	$(7.3 \pm 0.4) \times 10^6$	$(8.9 \pm 0.3) \times 10^{-3}$	$(3.6 \pm 0.2) \times 10^{-1}$	$(5.3 \pm 0.2) \times 10^6$
Br	0.92	$(3.6 \pm 0.2) \times 10^5$	$(4.1 \pm 0.2) \times 10^{-3}$	$(4.6 \pm 0.3) \times 10^{-1}$	$(3.3 \pm 0.2) \times 10^5$
CN	1.15	$(6.2 \pm 0.2) \times 10^2$	$(3.9 \pm 0.2) \times 10^{-4}$	1.2 ± 0.1	$(1.5 \pm 0.1) \times 10^3$

[a] The K_0 values were determined by the UV−vis spectral titration of X-DMA with Sc^{3+}. [b] Rate constants in the absence of Sc^{3+}. [c] Rate constants determined in the presence of 15 mM of Sc^{3+}. [d] Rate constants of reactions of $[Fe^{IV}(O)(N4Py)]^{2+}$ with free X-DMA which is not bound to Sc^{3+}, determined by eq 6, when the concentration of free Sc^{3+} ($[Sc^{3+}]_0 - [X\text{-}DMA]_0$) is 10 mM.[42]

dx.doi.org/10.1021/ic201545a |*Inorg. Chem.* 2011, 50, 11612–11622

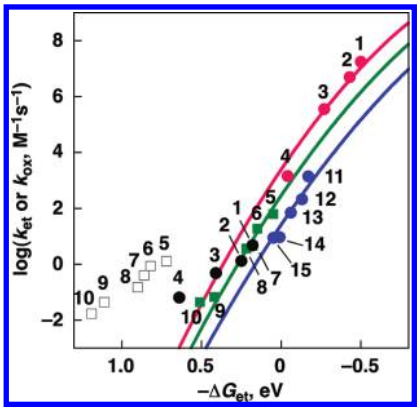

Figure 8. Plots of log k_{et} for electron transfer from X-DMA (X = Me for 1, H for 2, Br for 3, CN for 4) to $[Fe^{IV}(O)(N4Py)]^{2+}$ in the absence of Sc^{3+} (closed black circles) and in the presence of free Sc^{3+} (10 mM, closed pink circles) in MeCN at 298 K vs the driving force of electron transfer $[-\Delta G_{et} = e(E_{red} - E_{ox})]$ from X-DMA to $[Fe^{IV}(O)(N4Py)]^{2+}$. Squares show the driving force dependence of rate constants (log k_{ox} for oxygenation reaction of *para*-X-substituted thioanisoles (X = Me for 5, H for 6, Cl for 7, Br for 8, CN for 9, NO_2 for 10) by $[Fe^{IV}(O)(N4Py)]^{2+}$ in the absence of Sc^{3+} (open black squares) and in the presence of Sc^{3+} (10 mM, closed green squares) in MeCN at 298 K. Closed blue circles show the driving force dependence of rate constants (log k_{et}) for electron transfer from one-electron reductants (11, $[Fe^{II}(Ph_2\text{-Phen})_3]^{2+}$; 12, $[Fe^{II}(bpy)_3]^{2+}$; 13, $[Ru^{II}(Me_2\text{-bpy})_3]^{2+}$; 14, $[Fe^{II}(Cl\text{-phen})_3]^{2+}$; 15, $[Ru^{II}(bpy)_3]^{2+}$) to $[Fe^{IV}(O)(N4Py)]^{2+}$ in the presence of Sc^{3+} (10 mM). The fitting to the Marcus theory of the electron transfer are shown by the pink line with λ = 1.79 eV, green line with λ = 2.02 eV and blue line with λ = 2.27 eV, respectively.

electron transfer from DMA and DMA-d_6 to $[Fe^{IV}(O)(N4Py)]^{2+}$ is the rate-determining step.

CONCLUSION

Rates of oxidation of X-DMA with $[Fe^{IV}(O)(N4Py)]^{2+}$ were significantly accelerated by the presence of $Sc(OTf)_3$ in MeCN at 298 K. In the case of DMA, the demethylation of DMA occurs via electron transfer from DMA to $[Fe^{IV}(O)(N4Py)]^{2+}$, followed by proton transfer from $DMA^{\bullet+}$ to $[Fe^{III}(O)(N4Py)]^{+}$. The initial electron transfer is remarkably accelerated by Sc^{3+} ion-coupled electron transfer. However, the subsequent proton transfer is prohibited by the binding of Sc^{3+} to $[Fe^{III}(O)(N4Py)]^{+}$, when $DMA^{\bullet+}$ dimerizes to form TMB, which is further oxidized by $[Fe^{IV}(O)(N4Py)]^{2+}$ to yield $TMB^{\bullet+}$ as the final three-electron oxidized product. When *para*-substituted DMA derivatives (X-DMA: X = Me, Br, CN) are employed, the initial electron transfer is also remarkably accelerated by Sc^{3+} ion-coupled electron transfer. The resulting $X\text{-}DMA^{\bullet+}$ cannot dimerize because of the blockage of the *para*-position, leading to the demethylation. The complicated kinetics of Sc^{3+} ion-coupled electron transfer from X-DMA to $[Fe^{IV}(O)(N4Py)]^{2+}$ is well analyzed by the competition of binding of Sc^{3+} to X-DMA and $[Fe^{IV}(O)(N4Py)]^{2+}$. The rate constants of Sc^{3+} ion-coupled electron transfer from uncomplexed X-DMA to $[Fe^{IV}(O)(N4Py)]^{2+}$, which were evaluated using the binding constants (K_0) of Sc^{3+} to X-DMA, agree well with those predicted by the Marcus plot of the rate constants of Sc^{3+} ion-coupled electron transfer from one-electron reductants to $[Fe^{IV}(O)(N4Py)]^{2+}$. Thus, the present study provides a general way to enhance the reactivity of high-valent metal-oxo species by binding of redox-inactive metal ions such as Sc^{3+} toward substrates which also bind with metal ions.

ASSOCIATED CONTENT

Supporting Information. Table S1 and Figures S1−S16. This material is available free of charge via the Internet at http://pubs.acs.org.

AUTHOR INFORMATION

Corresponding Author

*E-mail: fukuzumi@chem.eng.osaka-u.ac.jp (S.F.), wwnam@ewha.ac.kr (W.N.).

ACKNOWLEDGMENT

The research at OU was supported by Grant-in-Aid (No. 19205019 to S.F.) and Global COE program, "the Global Education and Research Center for Bio-Environmental Chemistry" from the Ministry of Education, Culture, Sports, Science and Technology, Japan (to S.F.) and the research at EWU was supported by NRF/MEST of Korea through CRI (to W.N.), GRL (2010-00353) (to W.N.), 2011 KRICT OASIS project (to W.N.), and WCU (R31-2008-000-10010-0) (to W.N. and S.F.).

REFERENCES

(1) (a) Ortiz de Montellano, P. R. *Cytochrome P450: Structure, Mechanism, and Biochemistry*, 3rd ed.; Kluwer Academic/Plenum Publishers: New York, 2005. (b) Meunier, B., Ed.; *Biomimetic Oxidations Catalyzed by Transition Metal Complexes*; Imperial College Press: London, 2000. (c) *The Ubiquitous Role of Cytochrome P450 Proteins In Metal Ions in Life Sciences*; Sigel, A., Sigel, H., Sigel, R. K. O., Eds.; John Wiley & Sons Ltd: Chichester, England, 2007; Vol. 3.

(2) (a) Sono, M.; Roach, M. P.; Coulter, E. D.; Dawson, J. H. *Chem. Rev.* **1996**, *96*, 2841. (b) Watanabe, Y. *J. Biol. Inorg. Chem.* **2001**, *6*, 846. (c) Jung, C. *Biochim. Biophys. Acta* **2011**, *1814*, 46.

(3) (a) Groves, J. T.; Shalyaev, K.; Lee, J. In *The Porphyrin Handbook*; Kadish, K. M., Smith, K. M., Guilard, R., Eds.; Academic Press: Elsevier Science: New York, 2000; Vol. 4, pp 17−40. (b) Watanabe, Y. In *The Porphyrin Handbook*; Kadish, K. M., Smith, K. M., Guilard, R., Eds.; Academic Press: Elsevier Science (USA), 2000, Vol. 4, pp 97−117. (c) Groves, J. T. *J. Inorg. Biochem.* **2006**, *100*, 434.

(4) (a) Meunier, B.; de Visser, S. P.; Shaik, S. *Chem. Rev.* **2004**, *104*, 3947. (b) Shaik, S.; Cohen, S.; Wang, Y.; Chen, H.; Kumar, D.; Thiel, W. *Chem. Rev.* **2010**, *110*, 949. (c) Abu-Omar, M. M.; Loaiza, A.; Hontzeas, N. *Chem. Rev.* **2005**, *105*, 2227. (d) Denisov, I. G.; Makris, T. M.; Sligar, S. G.; Schlichting, I. *Chem. Rev.* **2005**, *105*, 2253. (e) Ortiz de Montellano, P. R. *Chem. Rev.* **2010**, *110*, 932.

(5) (a) Krebs, C.; Fujimori, D. G.; Walsh, C. T.; Bollinger, J. M., Jr. *Acc. Chem. Res.* **2007**, *40*, 484. (b) Que, L., Jr. *Acc. Chem. Res.* **2007**, *40*, 493. (c) Nam, W. *Acc. Chem. Res.* **2007**, *40*, 522. (d) Borovik, A. S. *Acc. Chem. Res.* **2005**, *38*, 54. (e) Shaik, S.; Lai, W.; Chen, H.; Wang, Y. *Acc. Chem. Res.* **2010**, *43*, 1154.

(6) (a) Comba, P.; Kerscher, M.; Schiek, W. *Prog. Inorg. Chem.* **2007**, *55*, 613. (b) Bakac, A. *Coord. Chem. Rev.* **2006**, *250*, 2046. (c) Espenson, J. H. *Coord. Chem. Rev.* **2005**, *249*, 329. (d) Fujii, H. *Coord. Chem. Rev.* **2002**, *226*, 51.

(7) (a) Costas, M.; Mehn, M. P.; Jensen, M. P.; Que, L., Jr. *Chem. Rev.* **2004**, *104*, 939. (b) Tshuva, E. Y.; Lippard, S. J. *Chem. Rev.* **2004**, *104*, 987. (c) Que, L., Jr.; Ho, R. Y. N. *Chem. Rev.* **1996**, *96*, 2607. (d) Solomon, E. I.; Brunold, T. C.; Davis, M. I.; Kemsley, J. N.; Lee, S.-K.; Lehnert, N.; Neese, F.; Skulan, A. J.; Yang, Y.-S.; Zhou, J. *Chem. Rev.* **2000**, *100*, 235. (e) Decker, A.; Solomon, E. I. *Curr. Opin. Chem. Biol.* **2005**, *9*, 152.

(8) (a) Yiu, S.-M.; Man, W.-L.; Lau, T.-C. *J. Am. Chem. Soc.* **2008**, *130*, 10821. (b) Lam, W. W. Y.; Yiu, S.-M.; Lee, J. M. N.; Yau, S. K. Y.; Kwong, H.-K.; Lau, T.-C.; Liu, D.; Lin, Z. *J. Am. Chem. Soc.* **2006**, *128*, 2851. (c) Yiu, S.-M.; Wu, Z.-B.; Mak, C.-K.; Lau, T.-C. *J. Am. Chem. Soc.* **2004**, *126*, 14921. (d) Miller, C. G.; Gordon-Wylie, S. W.; Horwitz, C. P.; Strazisar, S. A.; Peraino, D. K.; Clark, G. R.; Weintraub, S. T.; Collins, T. J. *J. Am. Chem. Soc.* **1998**, *120*, 11540.

(9) (a) Fukuzumi, S.; Morimoto, Y.; Kotani, H.; Naumov, P.; Lee, Y.-M.; Nam, W. *Nat. Chem.* **2010**, *2*, 756. (b) Karlin, K. D. *Nat. Chem.* **2010**, *2*, 711.

(10) Morimoto, Y.; Kotani, H.; Park, J.; Lee, Y.-M.; Nam, W.; Fukuzumi, S. *J. Am. Chem. Soc.* **2011**, *133*, 403.

(11) Park, J.; Morimoto, Y.; Lee, Y.-M.; Nam, W.; Fukuzumi, S. *J. Am. Chem. Soc.* **2011**, *133*, 5236.

(12) (a) Fukuzumi, S. *Prog. Inorg. Chem.* **2009**, *56*, 49. (b) Fukuzumi, S. *Bull. Chem. Soc. Jpn.* **1997**, *70*, 1. (c) Fukuzumi, S.; Ohtsu, H.; Ohkubo, K.; Itoh, S.; Imahori, H. *Coord. Chem. Rev.* **2002**, *226*, 71. (d) Fukuzumi, S.; Ohkubo, K. *Coord. Chem. Rev.* **2010**, *254*, 372. (e) Fukuzumi, S.; Itoh, S. *Antioxid. Redox Signaling* **2001**, *3*, 807.

(13) (a) Fukuzumi, S.; Kuroda, S.; Tanaka, T. *J. Am. Chem. Soc.* **1985**, *107*, 3020. (b) Itoh, S.; Taniguchi, M.; Takada, N.; Nagatomo, S.; Kitagawa, T.; Fukuzumi, S. *J. Am. Chem. Soc.* **2000**, *122*, 12087. (c) Fukuzumi, S.; Yasui, K.; Suenobu, T.; Ohkubo, K.; Fujitsuka, M.; Ito, O. *J. Phys. Chem. A* **2001**, *105*, 10501.

(14) (a) Fukuzumi, S.; Ohkubo, K. *Chem.—Eur. J.* **2000**, *6*, 4532. (b) Fukuzumi, S.; Ohkubo, K. *J. Am. Chem. Soc.* **2002**, *124*, 10270. (c) Ohkubo, K.; Menon, S. C.; Orita, A.; Otera, J.; Fukuzumi, S. *J. Org. Chem.* **2003**, *68*, 4720.

(15) (a) Itoh, S.; Kumei, H.; Nagatomo, S.; Kitagawa, T.; Fukuzumi, S. *J. Am. Chem. Soc.* **2001**, *123*, 2165. (b) Fukuzumi, S.; Satoh, N.; Okamoto, T.; Yasui, K.; Suenobu, T.; Seko, Y.; Fujitsuka, M.; Ito, O. *J. Am. Chem. Soc.* **2001**, *123*, 7756. (c) Fukuzumi, S.; Ohkubo, K.; Okamoto, T. *J. Am. Chem. Soc.* **2002**, *124*, 14147.

(16) (a) Fukuzumi, S.; Okamoto, K.; Imahori, H. *Angew. Chem., Int. Ed.* **2002**, *41*, 620. (b) Okamoto, K.; Imahori, H.; Fukuzumi, S. *J. Am. Chem. Soc.* **2003**, *125*, 7014. (c) Fukuzumi, S.; Okamoto, K.; Yoshida, Y.; Imahori, H.; Araki, Y.; Ito, O. *J. Am. Chem. Soc.* **2003**, *125*, 1007. (d) Savéant, J.-M. *J. Am. Chem. Soc.* **2008**, *130*, 4732.

(17) (a) Chen, X.; Bu, Y. *J. Am. Chem. Soc.* **2007**, *129*, 9713. (b) Wu, H.; Zhang, D.; Su, L.; Ohkubo, K.; Zhang, C.; Yin, S.; Mao, L.; Shuai, Z.; Fukuzumi, S.; Zhu, D. *J. Am. Chem. Soc.* **2007**, *129*, 6839. (c) Zeng, Y.; Zhang, G.; Zhang, D.; Zhu, D. *J. Org. Chem.* **2009**, *74*, 4375. (d) Jia, L.; Zhang, G.; Zhang, D.; Xiang, J.; Xu, W.; Zhu, D. *Chem. Commun.* **2011**, *47*, 322.

(18) (a) Yuasa, J.; Suenobu, T.; Fukuzumi, S. *J. Am. Chem. Soc.* **2003**, *125*, 12090. (b) Yuasa, J.; Suenobu, T.; Fukuzumi, S. *ChemPhysChem* **2006**, *7*, 942. (c) Yuasa, J.; Yamada, S.; Fukuzumi, S. *Chem.—Eur. J.* **2008**, *14*, 1866.

(19) (a) Fukuzumi, S.; Koumitsu, S.; Hironaka, K.; Tanaka, T. *J. Am. Chem. Soc.* **1987**, *109*, 305. (b) Fukuzumi, S.; Kondo, Y.; Tanaka, T. *J. Chem. Soc., Perkin Trans. 2* **1984**, 673. (c) Fukuzumi, S.; Kondo, Y.; Tanaka, T. *Chem. Lett.* **1983**, 485.

(20) (a) Fukuzumi, S.; Nishizawa, N.; Tanaka, T. *J. Chem. Soc., Perkin Trans, 2* **1985**, 371. (b) Fukuzumi, S.; Fujii, Y.; Suenobu, T. *J. Am. Chem. Soc.* **2001**, *123*, 10191.

(21) (a) Miwa, G. T.; Walsh, J. S.; Kedderis, G. L.; Hollenberg, P. F. *J. Biol. Chem.* **1983**, *258*, 14445. (b) Guengerich, F. P.; Yun, C.-H.; Macdonald, T. L. *J. Biol. Chem.* **1996**, *271*, 27321. (c) Lindsay Smith, J. R.; Mortimer, D. N. *J. Chem. Soc., Perkin Trans. 2* **1986**, 1743.

(22) (a) Dinnocenzo, J. P.; Karki, S. B.; Jones, J. P. *J. Am. Chem. Soc.* **1993**, *115*, 7111. (b) Manchester, J. I.; Dinnocenzo, J. P.; Higgins, L.; Jones, J. P. *J. Am. Chem. Soc.* **1997**, *119*, 5069. (c) Karki, S. B.; Dinnocenzo, J. P.; Jones, J. P.; Korzekwa, K. R. *J. Am. Chem. Soc.* **1995**, *117*, 3657.

(23) (a) Goto, Y.; Watanabe, Y.; Fukuzumi, S.; Jones, J. P.; Dinnocenzo, J. P. *J. Am. Chem. Soc.* **1998**, *120*, 10762. (b) Goto, Y.; Matsui, T.; Ozaki, S.; Watanabe, Y.; Fukuzumi, S. *J. Am. Chem. Soc.* **1999**, *121*, 9497. (c) Fukuzumi, S.; Shimoosako, K.; Suenobu, T.; Watanabe, Y. *J. Am. Chem. Soc.* **2003**, *125*, 9074.

(24) (a) Shaffer, C. L.; Morton, M. D.; Hanzlik, R. P. *J. Am. Chem. Soc.* **2001**, *123*, 8502. (b) Bhakta, M. N.; Wimalasena, K. *J. Am. Chem. Soc.* **2002**, *124*, 1844. (c) Shaffer, C. L.; Harriman, S.; Koen, Y. M.; Hanzlik, R. P. *J. Am. Chem. Soc.* **2002**, *124*, 8268. (d) Bhakta, M.; Hollenberg, P. F.; Wimalasena, K. *Chem. Commun.* **2005**, 265. (e) Bhakta, N.; Hollenberg, P. F.; Wimalasena, K. *J. Am. Chem. Soc.* **2005**, *127*, 1376. (f) Bhakta, M. N.; Wimalasena, K. *Eur. J. Org. Chem.* **2005**, 4801. (g) Cerny, M. A.; Hanzlik, R. P. *J. Am. Chem. Soc.* **2006**, *128*, 3346.

(25) (a) Baciocchi, E.; Lanzalunga, O.; Lapi, A.; Manduchi, L. *J. Am. Chem. Soc.* **1998**, *120*, 5783. (b) Baciocchi, E.; Gerini, M. F.; Lanzalunga, O.; Lapi, A.; Lo Piparo, M. G. *Org. Biomol. Chem.* **2003**, *1*, 422.

(26) Baciocchi, E.; Bietti, M.; Lanzalunga, O.; Lapi, A.; Raponi, D. *J. Org. Chem.* **2010**, *75*, 1378.

(27) Nehru, K.; Seo, M. S.; Kim, J.; Nam, W. *Inorg. Chem.* **2007**, *46*, 293.

(28) (a) Shearer, J.; Zhang, C. X.; Hatcher, L. Q.; Karlin, K. D. *J. Am. Chem. Soc.* **2003**, *125*, 12670. (b) Wang, Y.; Kumar, D.; Yang, C.; Han, K.; Shaik, S. *J. Phys. Chem. B* **2007**, *111*, 7700. (c) Chiavarino, B.; Cipollini, R.; Crestoni, M. E.; Fornarini, S.; Lanucara, F.; Lapi, A. *J. Am. Chem. Soc.* **2008**, *130*, 3208.

(29) Lubben, M.; Meetsma, A.; Wilkinson, E. C.; Feringa, B.; Que, L., Jr. *Angew. Chem., Int. Ed.* **1995**, *34*, 1512.

(30) Armarego, W. L. F.; Chai, C. L. L. *Purification of Laboratory Chemicals*, 5th ed.; Butterworth Heinemann: Amsterdam, The Netherlands, 2003.

(31) *Organic Syntheses*; Saltzman, H., Sharefkin, J. G., Eds.; Wiley: New York, 1973; Vol. V, p 658.

(32) Kirchgessner, M.; Sreenath, K.; Gopidas, K. R. *J. Org. Chem.* **2006**, *71*, 9849.

(33) Mann, C. K.; Barnes, K. K. In *Electrochemical Reactions in Nonaqueous Systems*; Mercel Dekker: New York, 1970.

(34) For $DMA^{\bullet+}$ see: (a) Sumalekshmy, S.; Gopidas, K. R. *Chem. Phys. Lett.* **2005**, *413*, 294. (b) Murakami, M.; Ohkubo, K.; Fukuzumi, S. *Chem.—Eur. J.* **2010**, *16*, 7820. (c) Amada, I.; Yamaji, M.; Tsunoda, S.; Shizuka, H. *J. Photochem. Photobiol. A: Chem.* **1996**, *95*, 27. (d) Shida, T. In *Electronic Absorption Spectra of Radical Ions*; Elsevier: Amsterdam, The Netherlands, 1988; p 209.

(35) Akutagawa, T.; Saito, G. *Bull. Chem. Soc. Jpn.* **1995**, *68*, 1753.

(36) (a) Streeter, I.; Wain, A. J.; Thompson, M.; Compton, R. G. *J. Phys. Chem. B* **2005**, *109*, 12636. (b) Josephy, P. D.; Eling, T.; Mason, R. P. *J. Biol. Chem.* **1982**, *257*, 3669.

(37) (a) Siegman, H. In *Technique of Electroorganic Synthesis; Technique of Chemistry*; Weinberg, N. L., Ed.; John Wiley: New York, 1975; Vol. 5, Part II, pp 667−1056. (b) Sekiguchi, S.; Kobori, Y.; Akiyama, K.; Tero-Kubota, S. *J. Am. Chem. Soc.* **1998**, *120*, 1325.

(38) Fukuzumi, S.; Shimoosako, K.; Suenobu, T.; Watanabe, Y. *J. Am. Chem. Soc.* **2003**, *125*, 9074.

(39) The yield of DMB was also one-third of the initial concentration of $[Fe^{IV}(O)(N4Py)]^{2+}$ (Supporting Information, Figure S3).

(40) It should be noted that formation of $TMB^{\bullet+}$ is prohibited under the conditions such that concentrations of DMA are smaller than that of Sc^{3+}, because of the binding of Sc^{3+} to DMA (Supporting Information, Figure S4).

(41) The spectra measured with a stopped-flow spectrometer in Figure 3b become noisy as compared with those measured with a photodiode-array UV−vis spectrophotometer in Figure 3a. The scandium(III) triflate salt used in Figure 3b was completely soluble in MeCN.

(42) In the case of CN-DMA, concentration of free Sc^{3+} is 10.7 mM because of the relatively small K_0 value.

(43) (a) Marcus, R. A. *Annu. Rev. Phys. Chem.* **1964**, *15*, 155. (b) Marcus, R. A. *Angew. Chem., Int. Ed. Engl.* **1993**, *32*, 1111.

NOTE ADDED AFTER ASAP PUBLICATION

This paper was published on the Web on October 19, 2011. Due to a production error, the paper was published with several text and graphic errors throughout the paper. The corrected version was reposted on October 24, 2011.